

A Tale Twice Told: The Luminosity Profiles of the Sagittarius Tails

M.Niederste-Ostholt^{1*}, V. Belokurov¹, N.W. Evans¹

¹*Institute of Astronomy, Madingley Rd, Cambridge, CB3 0HA*

May 2011

ABSTRACT

The Sagittarius dwarf galaxy is the archetype of a tidally disrupting system. Both leading and trailing tails can be observed across at least 180 degrees of the sky and measurements of their luminosity density profiles have recently become available. Using numerical simulations, we explore the factors that control the appearance of such profiles.

We use two possible models for the Sgr progenitor. The first is a one-component Plummer model, which may represent either a dark matter free progenitor, or one in which pre-existing dark matter has already been largely stripped. The second is a two-component model in which the stars are represented by a Hernquist sphere embedded in a cosmologically modish Navarro-Frenk-White dark halo. Disruption of the models in the Milky Way galaxy provides us with two tellings of the tale of the formation of the Sgr stream. The initial disintegration of the baryons proceeds more slowly for the two-component models because of the protective cocoon of dark matter. Once this has been stripped, though, matters proceed apace. In both cases, the profiles after ~ 6 pericentric passages provide good matches to the observational data, but the tails are more extended for the two-component models.

The leading and trailing tails are symmetric at apocentre or pericentre. At other orbital phases, asymmetries are present, as tails are compressed as they approach apocentre and stretched out as they approach pericentre. There may exist density enhancements corresponding to such pile-ups which may be observable in current survey data. We re-visit the calculation of Niederste-Ostholt et al. (2010) and slightly revise upwards the luminosity of the Sgr progenitor to $9.9 - 14.4 \times 10^7 L_{\odot}$ based on insights from the simulations.

Key words: galaxies: dwarf galaxies – galaxies: individual (Sagittarius) – galaxies: simulations

1 INTRODUCTION

This paper provides two tellings of the tale of the Sagittarius (Sgr) galaxy.

Ever since its discovery (Ibata et al. 1995), the Sgr dwarf has been recognised as a touchstone of Galactic astronomy. It provides an ongoing example of the merging and accretion of galaxies, one of the fundamental processes through which structure is built in the Universe. It provides one of the best measures of the Galactic potential and mass, as its tidal debris can be traced to distances of possibly ~ 90 kpc (Newberg et al. 2003; Belokurov et al. 2006; Koposov et al. 2011). The disruption of Sgr and the spilling of its stars and globular clusters into the Galaxy provides a sizeable frac-

tion, perhaps as much as a quarter, of the entire stellar halo of the Milky Way by luminosity (using numbers from Bell et al. (2008) or Deason et al. (2011) and Niederste-Ostholt et al. (2010)).

Given its fundamental role, the disruption of the Sgr dwarf and the formation of its tidal tails has been a popular topic for detailed numerical investigations. Motivated by the proximity of the remnant to the Galactic centre, simulations as to the effect of Milky Way tides on Sgr began soon after its discovery (Johnston et al. 1995). The aims of subsequent simulations are largely threefold. First, some investigators concentrated on understanding the Sgr progenitor (e.g. Velazquez & White 1995; Ibata & Lewis 1998; Lokas et al. 2010). The work of Jiang & Binney (2000) nicely summarizes the degeneracy in the properties of the progenitor, with the then available data being compatible with a very

* E-mail:mno, vasily, nwe@ast.cam.ac.uk

broad range of masses and orbital histories. Secondly, there is a body of work that has studied what can be inferred about the structure of the Milky Way, particularly its dark halo. This though has not led to clear-cut conclusions on the shape of the dark halo which has been variously claimed as spherical, oblate, prolate or triaxial (e.g. Helmi 2004a,b; Johnston et al. 2005; Fellhauer et al. 2006; Law & Majewski 2010). Thirdly, some investigators have been concerned primarily with the properties of the debris itself, particularly as positions, kinematics and metallicities of presumed stream members have gradually become available from wide area surveys like 2MASS and SDSS (e.g. Johnston 1998; Martínez-Delgado et al. 2004; Law et al. 2005; Law & Majewski 2010).

Recently, Niederste-Ostholt et al. (2010) have used the extant 2MASS and SDSS survey data to produce luminosity density profiles of both the leading and trailing tails. By extrapolating the observed profiles both near the core and along the orbit, the luminosity of the undisrupted system can be determined. These profiles have not yet been explored by simulations. In this contribution, we provide with the aid of N-body models two re-tellings of the tale of the Sgr galaxy. We are interested in constraining the dark matter content of the progenitor, as well as understanding what controls the appearance of the tail luminosity profiles.

Section 2 is primarily technical and gives details of the set-up of the simulations together with the analyses performed on the output. Section 3 provides the first telling of the tale with simulations in which the dark matter shadows the light in the progenitor. Section 4 provides the second telling of the tale with dark matter dominated progenitors. Finally, we draw our conclusions in Section 5.

2 SET-UP AND ASSUMPTIONS

An N-body satellite is placed on an orbit in a static Milky Way-like potential consisting of a Miyamoto & Nagai (1975) disc ($M_d = 7.5 \times 10^{10} M_\odot$, radial scale length = 3.5 kpc, vertical scale length = 0.3 kpc), a Hernquist (1990) bulge ($M_b = 1.3 \times 10^{10} M_\odot$, scale radius = 1.2 kpc), and a spherically symmetric logarithmic halo (circular velocity 186 kms^{-1} , scale size 12 kpc). Similar potentials have been used before (see e.g. Johnston et al. 1999b; Law et al. 2005; Fellhauer et al. 2006).

We explore two possibilities for the progenitor Sgr. In the first telling of the tale, the satellite is represented by a Plummer sphere of characteristic lengthscale r_c composed of 10^6 particles. This single component approach follows many previous papers, including Law & Majewski (2010) who are able to reproduce a wide array of observations. This mass-follows-light model can be interpreted as representing either a situation in which all dark matter has been stripped before the baryons begin significant disruption, or in which the satellite had little dark matter to begin with. In the second telling, the Sgr galaxy is embedded in a dark matter halo. Specifically, we use a two-component model consisting of baryons distributed in a Hernquist sphere of lengthscale r_c embedded in an Navarro-Frenk-White (NFW) dark matter halo with lengthscale r_s (c.f. Fellhauer et al. 2007). In both tellings, the models are released in the same Milky Way potential with the same initial conditions. They have the same

characteristic lengthscale and mass for the baryonic component. Their initial mean velocity dispersions are different (namely $\sim 15 \text{ kms}^{-1}$ and $\sim 19 \text{ kms}^{-1}$), but they both have mean dispersions consistent with the observations (Ibata et al. 1997) at the timestep corresponding to the present-day epoch ($\sim 10 \text{ kms}^{-1}$ and $\sim 11 \text{ kms}^{-1}$ respectively).

The size and mass of Sgr prior to disruption can only be estimated. However, based on the luminosity determined in Niederste-Ostholt et al. (2010), a mass of at least $10^8 M_\odot$ for the baryonic component is justifiable. Although we will consider the effects of the satellite mass and size on the shape of the luminosity profiles, our benchmark one and two-component models have a baryonic mass of $6.4 \times 10^8 M_\odot$ and a characteristic radius $r_c = 850 \text{ pc}$ (c.f. Law & Majewski 2010).

The evolution of the satellite as it tidally disrupts is followed by looking at snap-shots of the particle distribution at various locations along the orbit. The disruption is simulated with the particle-mesh code **SuperBox** (Fellhauer et al. 2000). For one-component models, it uses three nested grids of 64^3 cells each centred on the highest density region of the satellite galaxy. The inner high-resolution grid covers the central region of the satellite with the grid spanning $2 \times r_c$. The medium resolution grid covers the entire satellite ($10 \times r_c$). The low resolution grid covers $65 \times R_{\text{cutoff}}$, where $R_{\text{cutoff}} = 5r_c$ is the artificial cut-off radius imposed on the initial distribution of the dwarf galaxy. The simulation steps forward with a constant time-step size of $\Delta t = 1.3 \text{ Myr}$, which leads to a total energy conservation better than 1% when the satellite is evolved in isolation for $\sim 10 \text{ Gyr}$. For the two-component models, there are two sets of grids – the first covering the baryons and the second the dark matter particles. The sizes are set up relative to the baryonic characteristic scale r_c and the NFW scale radius r_s in an analogous way to the one-component models.

The orbit has initial conditions $(x, y, z) = (0, 0, 55) \text{ kpc}$ and $(u, v, w) = (90, 0, 0) \text{ kms}^{-1}$ which result in a pericentre of $\approx 15 \text{ kpc}$ and an apocentre $\approx 55 \text{ kpc}$ in line with observations of Sgr (e.g. Ibata & Lewis 1998; Johnston et al. 1999a; Ibata et al. 2001; Law et al. 2005). Radial and transverse velocity measurements of the main body of Sgr, as well as 2MASS observations of the trailing arm, indicate that the Sgr dwarf is currently located close to pericentre. The orbital period is approximately 0.7 Gyr. During each period, eight snapshots are taken in equally spaced time-steps, chosen so that one snap-shot is at apocentre and one at pericentre. The orbit lies in the plane perpendicular to the galactic disk, which makes the subsequent analysis considerably more straightforward. Observations of Sgr debris support the notion that the material torn from the satellite is confined to a plane (Majewski et al. 2003), with an orbital pole at $(\ell, b) = (273.8^\circ, -13.5^\circ)$ i.e. only slightly inclined from the plane used in this analysis. Our aim is not to reproduce exactly the orbit of the Sgr galaxy, but to obtain systems close enough so as to explore the luminosity profiles of the tails.

Particles are defined as bound, or unbound, depending on whether their kinetic energy exceeds, or not, the satellite's internal potential energy determined by **SuperBox**. Leading and trailing arm particles are then selected based on their orbital energies relative to the orbit of the centre of mass. In the inner regions of the satellite, approximately

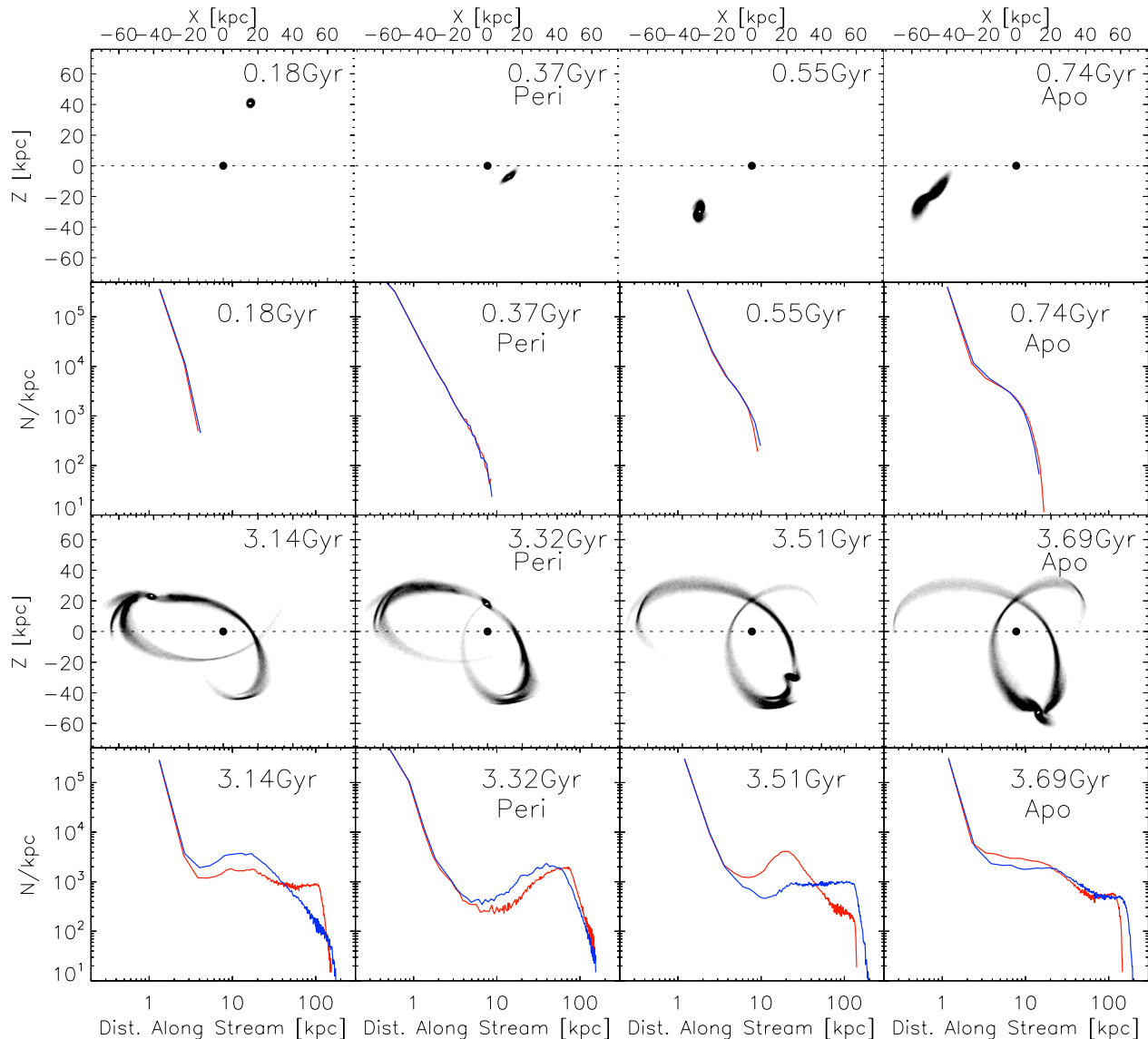


Figure 1. Snapshots and profiles of a typical simulation looking face-on into the orbital plane. The satellite has a Plummer radius 350 pc and mass $10^8 M_{\odot}$. The plots run forward in time from left to right and top to bottom. The dot shows the Galactic centre, which is centre of the Cartesian axes (X, Z) with $Z = 0$ defining the Galactic plane. The profiles represent the number density of particles along the stream with the leading arm in red and the trailing arm in blue. The early evolution of the satellite and its accompanying profiles are shown in the top two rows. The leading and trailing tails begin forming symmetrically and the profiles lie on top of each other. The bottom two rows show the later evolution of the satellite. Asymmetries begin to occur as the tails fill appreciable portions of the orbital path, between apocentre and pericentre. Overdensities occur as stars slow down near apocentre and the tail is compressed, whereas lower density areas occur the the tail is approaching pericentre and is stretched out. The profiles remain symmetric when Sgr is observed at either apocentre or pericentre. Asymmetries between the leading and trailing arms appear when Sgr is at intermediate positions along its orbit.

one half of the bound particles are assigned to the leading arm and one half to the trailing arm. The profiles are constructed in a fashion analogous to that used in Niederste-Ostholt et al. (2010) counting stars from a given arm in angular bins covering 1.2° on the sky. The bin size is chosen to have sufficient resolution along the tails whilst avoiding significant bin-to-bin variations. The counts are normalised by the length along the stream that is covered by a given bin and corrected for the angle that the stream makes with the radial direction at that location.

In addition, we require that the one-component progenitor has lost $\sim 60\%$ of its mass, as suggested in Niederste-Ostholt et al. (2010), which allows us to identify the appropriate pericentric passage (the sixth) to match to the present-day data. The timescale over which the disruption is followed is 4.1 Gyrs. The two-component model is allowed to evolve through the same number of pericentric passages, and loses $\sim 70\%$ of its mass along the way. As it evolves onto a tighter orbit, the time to the sixth pericentric passage is slightly shorter at 3.6 Gyrs.

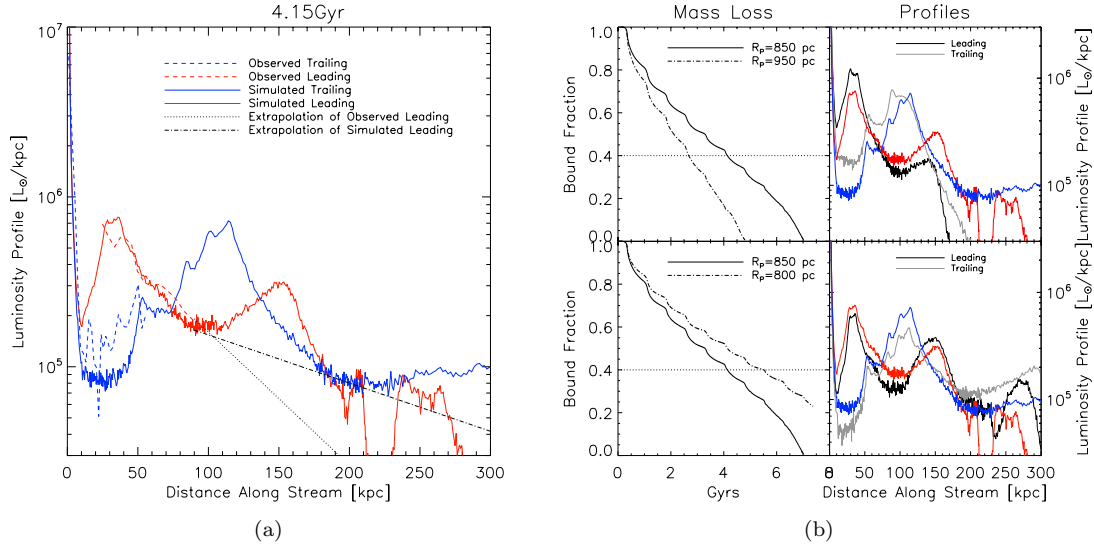


Figure 2. (a): Leading (red) and trailing (blue) arm profiles after 4.15 Gyr for the satellite used by Law & Majewski (2010) with $(M, r_c) = 6.4 \times 10^8 M_\odot, 850$ pc. The snapshot is taken after passing pericentre and the satellite has lost $\sim 60\%$ of its stars. The agreement between the simulated profiles (full lines) and observations (dashed lines) is good though the trailing arm appears slightly worse than the leading arm due to the log-scale). The short-dash dotted line shows the extrapolation used in Niederste-Ostholt et al. (2010). The long-dash dotted line shows an extrapolation based on the simulated profile, leaving out the additional bump in the profile. Niederste-Ostholt et al. (2010) may have underestimated the amount of light not seen in the leading arm by as much as 80%, though this does not change the luminosity range proposed for the progenitor Sgr since the extrapolation accounts for only a minor fraction of the total luminosity. (b): Varying the size of progenitor results in a poorer match with the observations, as changing the density of the progenitor influences how quickly stars disperse along the orbit. The left-hand column shows the mass-loss history of a satellite with $r_c = 950$ pc (top) and 800 pc (bottom), both with mass $6.4 \times 10^8 M_\odot$, compared to the benchmark satellite. The right hand column shows the corresponding density profiles when the satellite has lost 60% of its mass. The benchmark model is in red or blue (leading or trailing) whilst the larger and smaller scalelength models are in grey. There are noticeable differences in the density distribution.

3 THE FIRST TELLING

3.1 Luminosity Profiles of the Streams

Figure 1 shows snap-shots from a typical disruption of the one-component model, as well as the corresponding density profile along the stream. During the initial phase of the disruption, leading and trailing arms look very similar and their density profiles lie very nearly on top of each other. As the disruption proceeds and the progenitor and debris travel around the orbit, the leading and trailing arms develop differently, having different lengths and densities in a given snap shot.

The apocentric distances of the leading and trailing arm debris are approximately 44 kpc and 80 kpc respectively. These differences can be attributed to the different speeds with which unbound particles travel at various locations along the orbit (see e.g. Dehnen et al. 2004; Küpper et al. 2010) and the offset in energy between the leading and trailing arms relative to the orbit of the centre of mass. On a given orbit, particles close to pericentre travel fastest resulting in lower densities and more stretched out tidal streams. By contrast, particles spend more time near apocentre and the tails appear compressed and have higher densities. This can be seen, for example, in the snapshots at 3.51 Gyr which are taken when the main body of the progenitor has just passed its orbital pericentre (at 3.32 Gyr). The leading arm is approaching the next apocentre and is compressed. The trailing arm particles on the other hand have just left the

previous apocentre and are speeding up as they move towards pericentre, and thus have a lower density. This is consistent with the observed shape of the Sgr luminosity density profile, where the leading arm has a significantly higher density than the trailing arm (see Figure 10 of Niederste-Ostholt et al. 2010).

A progenitor with a different mass or size will, on a given orbit, disrupt at a different rate and the resulting debris will spread along the orbit with a different speed, depending on its tidal radius at pericentre, which controls the scale over which the satellite loses mass (Johnston et al. 2001). At fixed r_c (and in an identical host Galactic potential), a more massive progenitor loses mass more slowly, as it is more tightly bound. However, the unbound particles disperse along the orbit quicker, allowing the tails to grow longer, due to the larger spread in energies in the unbound particles. The slower mass-loss and quicker dispersion result in a lower density.

If identical one-component satellites are placed on different orbits with the same pericenter, then the debris spreads out over larger distances before reaching orbital turning points if the apocentre is larger. So, more eccentric orbits generally have a lower density, since the debris spreads out over a longer orbital path before being compressed at apocentre.

Figure 2a compares the observed profiles (dashed lines) to the simulated profiles produced by disrupting of the Law & Majewski (2010) Plummer sphere. The number of parti-

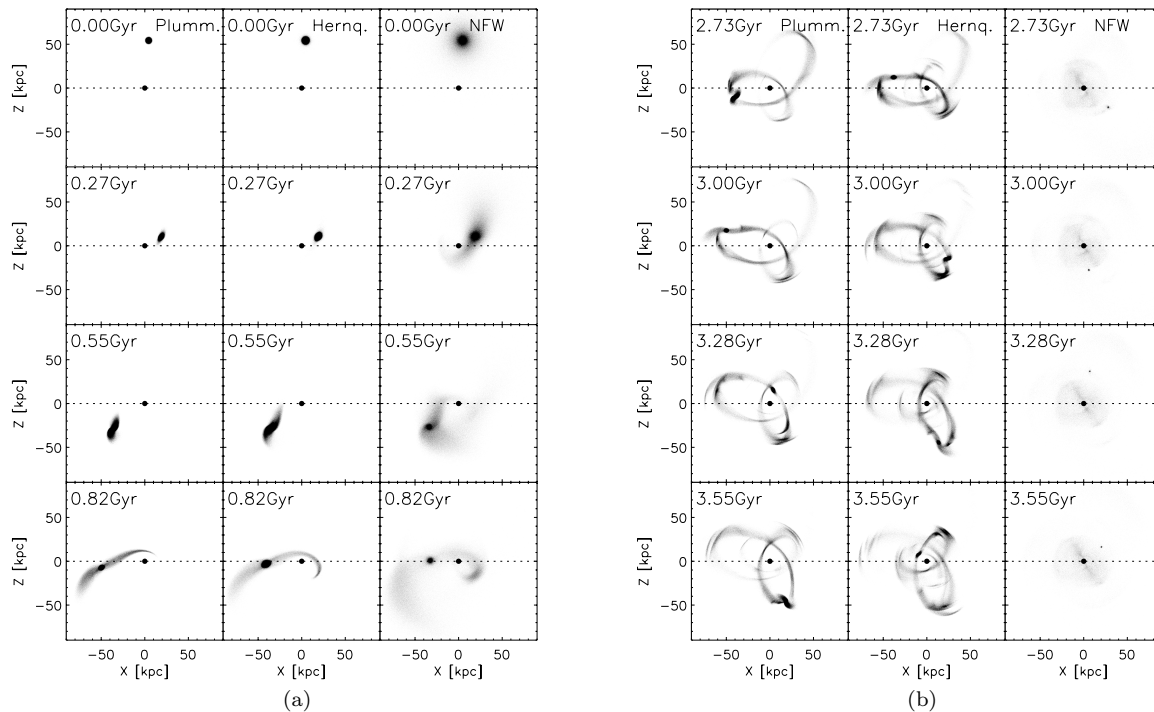


Figure 3. A comparison between the disruption of the one and two-component models (a) for the first 0.8 Gyrs and (b) at late times. The plots run forward in time from left to right and top to bottom. In both panels, the left-hand column shows the one-component Plummer sphere disrupting in a Milky Way potential. The middle column shows the baryonic component of the two-component model, whilst the right-hand column shows the evolution of the dark matter component. The extended dark matter begins disrupting immediately. Compared to the one-component model, the baryons in the two-component model at first disrupt more slowly. This results in lower density, longer tails — compare, for example, the baryonic material in the two component model with the one-component model at 082 Gyr. However, once a significant fraction of the protecting dark matter is removed, the baryonic disruption accelerates.

cles is converted to luminosities by assuming $M/L = 3.2$. This implies that the progenitor’s total luminosity is $\approx 2 \times 10^8 L_\odot$, which is at the higher end of the range determined by Niederste-Ostholt et al. (2010). The behaviour of the observed leading and trailing arms is well reproduced by the simulations. Figure 2b shows, progenitors with the same total mass, but with different sizes ($800 \text{ pc} < r_c < 950 \text{ pc}$), yield profiles that are different from our best-fit model. Consequently, there is significant disagreement with the observed profiles.

The leading and trailing arms have very nearly the same number of particles throughout the simulations. According to Choi et al. (2007), the self-gravity of the disrupting satellite can lead to asymmetries in the amount of material in the leading and trailing arms. However, our Sgr models are at the low-mass end of the satellites considered by Choi et al. (2007) and hence are unlikely to display much asymmetry between the leading and trailing arms. We conclude that calculating the total luminosity of Sgr progenitor based on measuring the luminosity of one tail only (as done in Niederste-Ostholt et al. 2010) does not introduce substantial error.

The observed asymmetry in density between the leading and trailing arms can be attributed to the phase of the orbit at the time of observation. Shortly after pericentre, part of the leading arm is compressed as it approaches the next orbital apocentre. The trailing arm on the other hand is stretched out as its particles are still approaching pericen-

tre. There is a pile-up in the trailing arm, stemming from particles at the previous apocentre.

The time taken to populate the stream ($\sim 4 \text{ Gyr}$) is in reasonable agreement with other predictions of the age of the debris (Law et al. 2005; Law & Majewski 2010). This is not surprising, since the satellite and potential are essentially the same as that of the Law et al. simulations. The simulations of Lokas et al. (2010) find a significantly shorter disruption time at 1.25 Gyr. This difference likely arises because they focus on reproducing the properties of the core of the progenitor rather than the tidal streams. As the authors highlight, the shorter interaction timescale is not necessarily in conflict with the longer interaction times required to form the tidal tails, but rather suggests that the length of time over which the Sgr core has been tidally stirred is relatively short.

3.2 The Assumptions of Niederste-Ostholt

Niederste-Ostholt et al. (2010) reassembled the stars in the Sgr remnant and tidal streams to estimate the luminosity of the Sgr progenitor. They found that the luminosity is in the range $(9.6\text{-}13.2) \times 10^7 L_\odot$ or $M_V - 15.1$ to -15.5 , making the Sgr progenitor comparable to, but somewhat less luminous than, the present-day Small Magellanic Cloud.

However, Niederste-Ostholt et al. (2010) made several assumptions, particularly at locations where stream data

was sparse or unavailable. These assumptions can now be tested using the N-body models. They include: (i) the behaviour of the leading arm near the core where it is obscured by the Galactic disc; (ii) the extrapolation of the leading arm beyond where it is observed in the SDSS data; and (iii) the rising density of the trailing arm after an initial drop resulting from the assumed metallicity gradient between the core and tails. In this section, we comment on each of these assumptions based on our simulations.

An important open question that remained in the observed profile of Sgr is the behaviour of the leading arm in the region where it is obscured by the Milky Way disk. This is the region at a distance along the stream less than ≈ 20 kpc in Figure 2a where the observations of the leading arm (red dashed line) end. From these simulations, it seems much more likely that the leading arm profile of Sgr dips down and joins the trailing arm profile near its minimum, rather than a continuing exponential rise suggested by the limited observations. This is borne out in other progenitor models ($175 \text{ pc} < r_c < 700 \text{ pc}$, $10^7 < M < 10^9 M_\odot$) and other orbits with pericentre at 15 kpc but apocentric distances between 35-100 kpc. Based on the drop in density and the obscuring influence of the Galactic disk, it will be challenging to detect this portion of the leading arm.

In Figure 2a, the leading arm follows an exponential decay save for another bump in the profile occurring at the apocentre an orbit ahead of the current location. If we look only at the extrapolated portion of the tail (distance > 100 kpc), then including the bump increases the amount of light by 70% over the exponential extrapolation. However, since the extrapolated portion of the profile contains relatively little light, the total luminosity in the tail changes only by 5% when integrating the extrapolated profile versus integrating the actual profile, indicating that ignoring the additional bump has only a small effect. The amount of light in the extrapolated portion of the tail is much more sensitive to the slope chosen. The exponential decline of the leading arm assumed in the determination of the total luminosity of Sgr may have been too steep. Employing a shallower extrapolation of the leading arm profile increases the total amount of light in the extrapolated portion of the leading arm by as much as $\sim 80\%$. Including a correction for the bump at ~ 150 kpc along the stream adds another $\sim 25\%$.

Concerning the trailing arm, Majewski et al. (2003) found their density profile based on 2MASS M-Giants to be flat. By contrast, Niederste-Ostholt et al. (2010) found the trailing arm of the Sgr stream has a positive slope due to the population differences between the satellites core and tails reflected in the changing ratio of the number of M giants to total luminosity. This population difference indicates a possible metallicity or age gradient between different regions of the undisrupted dwarf. The existence of such a gradient is already observed by Chou et al. (2007) who find a mean metallicity difference of ~ 0.6 dex in $[\text{Fe}/\text{H}]$ between the core and the stream. The fact that the simulations reproduce this behavior suggests that the proposed population gradient is in fact an acceptable approximation. However, we also need to consider that the density of the trailing arm is increasing when moving away from the core due to the pile-up of particles at the previous apocentre in the orbit, towards which the end of the trailing arm is reaching. The discovery of a

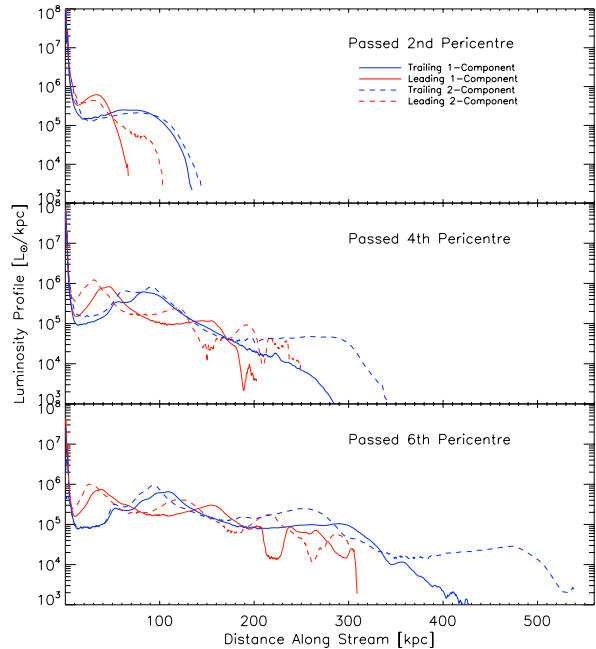


Figure 4. The luminosity profiles of the leading (red) and trailing (blue) tails for the one-component (solid lines) and two-component (dashed lines) models after (a) the second pericentric passage, (b) the fourth pericentric passage, and (c) the sixth pericentric passage. It is noticeable that at early times the two-component model is somewhat less dense than the one-component model, but has a much more extended central region and significantly longer tidal tails. After four pericentric passages, the densities are already very similar, though the two-component model has longer tails. Finally, after six pericentric passages even the density in the central region of the two-component satellite matches that of the one-component model closely. Slight differences remain along the profile resulting from the debris spreading farther along the orbit.

peak in density of the trailing arm followed by a drop would support this view.

Considering the insights gained from the simulations concerning the light in the leading arm farther than 100 kpc along the stream as well as the behaviour of the leading arm in the region obscured by the Galactic disk, *we can update the luminosity range for the Sgr system from $9.6 - 13.2 \times 10^7 L_\odot$ to $9.9 - 14.4 \times 10^7 L_\odot$.*

Within the uncertainties inherent in this approach, the luminosity range for Sgr has changed only slightly and the overwhelming factor controlling the spread remains the luminosity function assumed for Sgr and its debris (see Niederste-Ostholt et al. 2010, Figure 4.6).

4 THE SECOND TELLING

Dwarf galaxies show ample evidence of being dark matter dominated. So far our models have ignored the possibility that the stars visible from the Sgr galaxy were initially embedded in a dark matter halo. This motivates our second telling of the tale of the Sgr galaxy.

Using the code employed in Fellhauer et al. (2007), we generate a two-component galaxy consisting of baryons dis-

tributed in a Hernquist sphere embedded in an NFW dark matter halo. The two-component model is released in the Milky Way potential with the same initial conditions as the one-component model and luminosity profiles for the baryons are produced in the same fashion.

Specifically, the stellar distribution is represented by a Hernquist sphere of 10^6 particles. It has a mass of $6.4 \times 10^8 M_{\odot}$ and a scale radius of 850 pc, thus closely matching the Plummer model employed above. The NFW halo is represented by 5×10^5 particles with a scale radius of 3.5 kpc and a virial radius of 52.5 kpc. This concentration ($c \approx 15$) results in the baryonic component having a starting mean velocity dispersion of $\sim 19 \text{ kms}^{-1}$. This is larger than the initial velocity dispersion of the one-component model. As the disruption takes place, the mean velocity dispersion declines to a value that lies within the observational bounds at the present epoch.

Figure 3 shows the tidal evolution of the two model satellites considered in this paper. The left-hand column shows the one-component Plummer model for comparison purposes. The middle and right-hand columns show the evolution of the two-component model's baryonic and dark matter distributions respectively. Notice that the dark-matter NFW halo begins to disrupt immediately. The presence of dark matter increases the baryons' tidal radius. On the one hand, this initially inhibits the disruption of the baryonic component, when compared to the evolution of the Plummer model. However, the increased tidal radius translates into an increased energy spread in the debris. This results in thicker tails and stars dispersing faster along the orbit populating the tails out to longer distances. The dark matter halo quickly becomes significantly disrupted (after ca. two orbits) resulting in an accelerated rate of disruption of the baryonic component. This effect is increased by a slight orbital decay experienced by the two-component satellite once the dark-matter disrupts (the pericentre shrinks from ≈ 15 kpc to ≈ 11 kpc).

The leading and trailing tail profile shapes at the snapshots taken after the second, fourth, and sixth pericentric passage are shown in Figure 4. The sixth passage corresponds to the one chosen above as a comparison to the observations with Sagittarius. In this case, the final profiles of the two-component model look similar to those of the one-component model, albeit longer. Since the agreement between the profiles is good near the satellite core, the two-component and one-component models are almost indistinguishable based on the currently observed data.

Nonetheless, deeper data could distinguish between the profiles. The baryonic material in the two-component model starts off with a higher mean velocity dispersion than the one component-model ($\sim 19 \text{ kms}^{-1}$ as opposed to 15 kms^{-1}), though both remnants have essentially the same mean velocity dispersion at the end. This however means that the stars in the tails produced by the two-component model are moving on average somewhat faster and so the tails grow longer over the disruption timescale. At the present orbital phase, this is especially the case for the trailing arm. One possible discriminant between the models might be to search for this extended trailing tail using giant stars or blue horizontal branch stars.

There are also differences in the properties of the remnant, which is more compact and rounder in the two-

component model than the one-component, (though neither model is as flatted as the actual Sgr remnant). The ratio of initial to final baryonic mass within a 5 kpc aperture is 0.43 for the one-component case and 0.29 for the two component. This shows that more of the baryonic material is removed from the immediate vicinity of the Sgr remnant in the latter case.

5 DISCUSSION AND CONCLUSIONS

We have used the particle mesh-code **SuperBox** to disrupt models of the Sagittarius satellite in a Milky Way potential. As progenitors, we constructed N body representations with similar baryonic components, but with very different dark matter content. The one-component models mimic a situation in which any dark matter has been stripped from the dwarf galaxy prior to the disruption of the baryonic component, or in which the satellite had very little dark matter in the beginning. The two-component models have a baryonic component embedded within a cosmologically-inspired dark halo. Their disruption in the Milky Way potential provides two tellings of the tale of the formation of the Sgr galaxy and its tidal streams.

The stellar components are structurally indistinguishable at outset, having similar characteristic lengthscales and masses. They have different initial mean velocity dispersions, but this ensures that the remnant's final velocity dispersion lies within the present-day observational constraints. We have provided the first comparisons between simulation data and the observed luminosity density profiles of the leading and trailing Sgr tails constructed by Niederste-Ostholt et al. (2010).

Our main conclusions are

[1] The profiles of the tails can provide a strong constraint on the dark matter content of the Sgr system, though this requires deeper data than is currently available. The two-component model has longer tails than the one-component model. This is because the tidal radius and the starting mean velocity dispersion of the baryonic component in the two-component model are larger than that of the one-component model. Stars diffuse slightly more quickly along the tails, which as a consequence are longer and less dense. The length of the tails is an important discriminant. If we do observe very long tails for Sgr, then a one component model would need to be more massive to populate them to those distances. Even though there is some freedom to vary the (stellar) mass to light ratio by a factor of ~ 2 from our assumed value of 3.2, we have verified by simulations that this does not permit the present data on the tail length and profiles to be matched.

[2] One-component models successfully reproduce the density of the tails with only a baryonic component. Two-component models produce similar results within 180° of the remnant. Although the addition of a dark matter halo does initial protect the baryons from disruption, once the dark matter halo has been removed, the profiles develop in a similar fashion. With the present data, it is not possible to distinguish between one and two-component models based on fitting the profiles.

[3] The simulations support the idea that the amount of

light in the leading and trailing arms is nearly identical. The main reason for the difference in luminosity density between the leading and trailing arms observed in Sgr is the orbital phase at the present epoch. Shortly after pericentre, part of the leading arm is compressed as it approaches the next orbital apocentre. The trailing arm on the other hand is stretched out, as its particles are still approaching pericentre.

[4] The simulations have strengthened a number of the assumptions made by Niederste-Ostholt et al. (2010) in determining the total luminosity of the Sgr system. It is very likely that the leading arm's luminosity density, in the region where it is obscured by the Galactic disk, dips down to become symmetric with the trailing arm. Furthermore, the extrapolation of the leading arm's profile proposed in Niederste-Ostholt et al. (2010) is appropriate (with the possibility of a slightly different slope for the exponential decline), but requires the inclusion of additional light due to pile-ups at the next orbital apocentre. These factors lead to a slight upward revision of the total luminosity of the Sgr progenitor proposed by Niederste-Ostholt et al. (2010) to $9.9 - 14.4 \times 10^7 L_{\odot}$.

[5] The pile-ups of particles in the leading arm seems to be as dense as some parts of the already observed profile. Hence, it may be possible to detect these in existing survey data. Similarly, the increasing density of the trailing arm may allow further detections of that debris tail. The number of such density enhancements discovered may provide valuable constraints on the length of the tidal tails and the number of orbits over which the debris is spread. However, the highest density enhancements occur naturally around the apocentre of the orbits, which may be as far as 90 kpc from the observer in the case of the trailing arm (e.g., Koposov et al. 2011). This may render detection difficult with current surveys such as the SDSS. The highest overdensity in the leading arm, at a distance of ~ 47 kpc, has a main-sequence turn-off at $i \sim 21.4$. If we assume that turn-offs can be detected down to $i = 22$, this suggests that we may be able to detect such overdensities out to ~ 60 kpc using this approach. Other stream tracers, such as blue horizontal branch stars or M giants, may be observed out to greater distances.

ACKNOWLEDGMENTS

We thank the referee, David Law, for a careful reading of the paper and valuable comments. MNO thanks the Gates Cambridge Trust, the Isaac Newton Studentship fund and the Science and Technology Facilities Council (STFC), whilst VB acknowledges financial support from the Royal Society.

REFERENCES

- Bell E. F., Zucker D. B., Belokurov V., et al., 2008, *The Astrophysical Journal*, 680, 295
- Belokurov V., Zucker D. B., Evans N. W., et al., 2006, *The Astrophysical Journal*, 642, L137
- Choi J.-H., Weinberg M. D., Katz N., 2007, *Monthly Notices of the Royal Astronomical Society*, 381, 987
- Chou M.-Y., Majewski S. R., Cunha K., et al., 2007, *The Astrophysical Journal*, 670, 346
- Deason A. J., Belokurov V., Evans N. W., 2011, *MNRAS*, 416, 2903
- Dehnen W., Odenkirchen M., Grebel E. K., Rix H.-W., 2004, *The Astronomical Journal*, 127, 2753
- Fellhauer M., Belokurov V., Evans N. W., et al., 2006, *The Astrophysical Journal*, 651, 167
- Fellhauer M., Kroupa P., Baumgardt H., et al., 2000, *New Astronomy*, 5, 305
- Helmi A., 2004a, *Monthly Notices of the Royal Astronomical Society*, 351, 2, 643
- Helmi A., 2004b, *The Astrophysical Journal*, 610, L97
- Hernquist L., 1990, *Astrophysical Journal*, 356, 359
- Ibata R., Lewis G. F., Irwin M., Totten E., Quinn T., 2001, *The Astrophysical Journal*, 551, 294
- Ibata R. A., Gilmore G., Irwin M. J., 1995, *Monthly Notices RAS*, 277, 781
- Ibata R. A., Lewis G. F., 1998, *Astrophysical Journal* v.500, 500, 575
- Ibata R. A., Wyse R. F. G., Gilmore G., Irwin M. J., Suntzeff N. B., 1997, *Astronomical Journal* v.113, 113, 634
- Jiang I.-G., Binney J., 2000, *Monthly Notices of the Royal Astronomical Society*, 314, 468
- Johnston K. V., 1998, *Astrophysical Journal* v.495, 495, 297
- Johnston K. V., Law D. R., Majewski S. R., 2005, *The Astrophysical Journal*, 619, 800
- Johnston K. V., Majewski S. R., Siegel M. H., Reid I. N., Kunkel W. E., 1999a, *The Astronomical Journal*, 118, 1719
- Johnston K. V., Sackett P. D., Bullock J. S., 2001, *The Astrophysical Journal*, 557, 137
- Johnston K. V., Sigurdsson S., Hernquist L., 1999b, *Monthly Notices of the Royal Astronomical Society*, 302, 771
- Johnston K. V., Spergel D. N., Hernquist L., 1995, *Astrophysical Journal* v.451, 451, 598
- Koposov S. E., Belokurov V., Evans N. W., et al., 2011, *ArXiv e-prints*
- Küpper A. H. W., Kroupa P., Baumgardt H., Heggie D. C., 2010, *Monthly Notices of the Royal Astronomical Society*, 401, 105
- Law D. R., Johnston K. V., Majewski S. R., 2005, *The Astrophysical Journal*, 619, 807
- Law D. R., Majewski S. R., 2010, *ApJ*, 714, 229
- Lokas E. L., Kazantzidis S., Majewski S. R., Law D. R., Mayer L., Frinchaboy P. M., 2010, *arXiv, astro-ph.CO*
- Majewski S. R., Skrutskie M. F., Weinberg M. D., Osthheimer J. C., 2003, *The Astrophysical Journal*, 599, 1082
- Martínez-Delgado D., Gómez-Flechoso M. Á., Aparicio A., Carrera R., 2004, *The Astrophysical Journal*, 601, 242
- Miyamoto M., Nagai R., 1975, *PASJ*, 27, 533
- Newberg H. J., Yanny B., Grebel E. K., et al., 2003, *The Astrophysical Journal*, 596, L191
- Niederste-Ostholt M., Belokurov V., Evans N. W., Peñarrubia J., 2010, *The Astrophysical Journal*, 712, 516
- Velazquez H., White S. D. M., 1995, *Monthly Notices of the Royal Astronomical Society*, 275, L23